Ultrafast Carotenoid to Retinal Energy Transfer in Xanthorhodopsin Revealed by the Combination of Transient Absorption and Two Dimensional Electronic Spectroscopy

Supporting Information

This PDF includes:

S1 Spectral Overlap using theoretical and measured CAR S_2 fluorescence

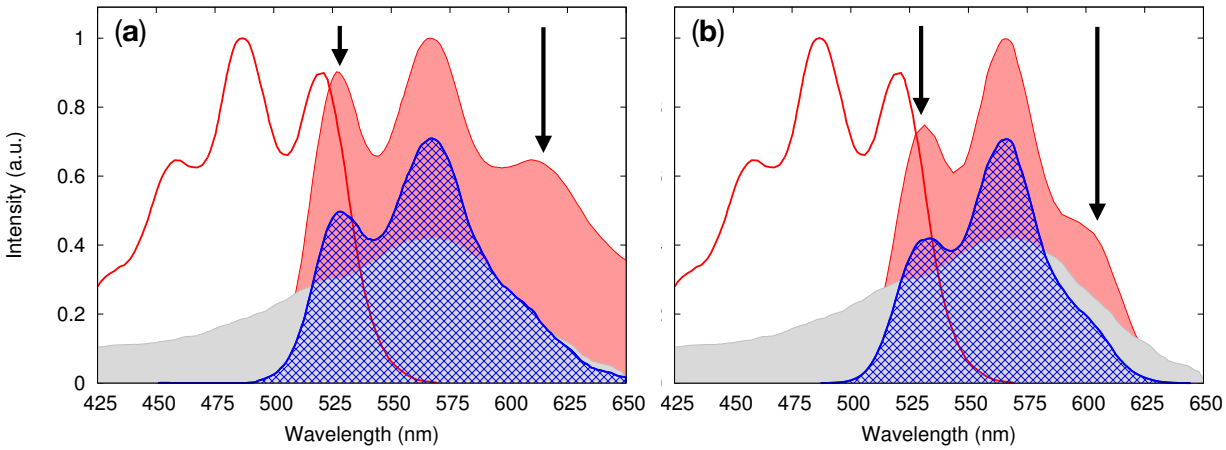

Figure S1: (a) Experimental absorption spectra of RXR (red solid line) and its mirror image, representing the fluorescence spectrum (red filled curve), together with RET absorption (grey filled curve). The Spectral Overlap is depicted in blue (same of Figure 2 in the main text). (b) Same of (a) employing the measured CAR S_2 fluorescence. The arrows indicate the regions in which the two fluorescence profiles differ significantly. Absorption and fluorescence spectra were adapted from ref. 2.

S2 XR scaling factor

As described in the main text, the analysis of the spectral overlap suggests that large percentage of the excited CAR molecules will not repopulate the original (cold) GS, but rather (hot) excited vibrational states of it. In particular, the area underneath the first peak of the spectral overlap (blue curves in Figure S1) gives an estimate of the percentage of molecules which will repopulate the ground vibrational state of the electronic CAR GS. In the main text we estimate it to be around 40%. Here we show that a variation of this value between 20% and 60% does not impact the main result described in the main text.

Figure S2 shows 2DES cuts of XR and RXR, taken averaging excitation wavelengths in the 515-530 nm interval. The different XR curves are obtained by renormalizing the XR data according to the estimated percentage of repopulation of the original CAR GS (20%, 40% and 60%), so that, at $t_2 \sim 400$ fs, the XR CAR GSB intensity (at the 520 nm diagonal) is the 92%, 85%, 76% of the RXR CAR GSB intensity. We observe that the excess of signal amplitude in the XR sample at the CAR-RET cross-peak, interpreted as the a direct signature of energy transfer, is preserved with all the employed scaling factors.

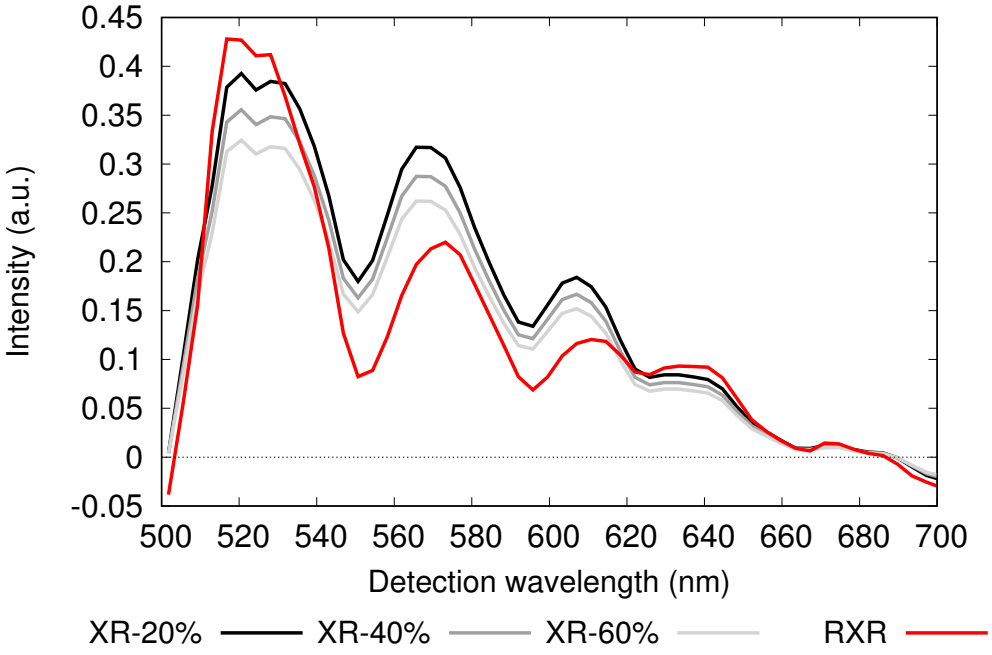

Figure S2: 2DES cuts of XR (black-grey solid line) and RXR (red solid line), obtained averaging excitations wavelengths in the 515-530 nm interval. Different XR curves correspond to different percentage of repopulation of the original CAR GS. An excess of signal amplitude in the XR sample (with respect to the RXR sample) at the CAR-RET cross-peak is always observed.

S3 The time-trace of the 560 nm signal

Figure S3 shows the comparison of XR and RXR signals, recorded at the diagonal (560 nm) along t_2. The average intensity of the XR signal ($\sim$0.065) is higher than that of the RXR signal ($\sim$0.025), as one expects direct RET contributions to appear in this spectral region in the XR sample.

If in the region in which the RET has the largest absorption (i.e., around 560 nm) the difference between XR and RXR is around $\sim$ 0.04 (in the given intensity scale), the observed difference of $\sim$ 0.1 (in the same intensity scale) observed at the CAR-RET cross peak, cannot be ascribed to sole direct RET contributions. We interprete the missing intensity as coming from energy transfer related RET signals, intensified by the fact that the first two dipole interactions involve the strongly absorbing CAR chromophore (as discussed in the following Section).

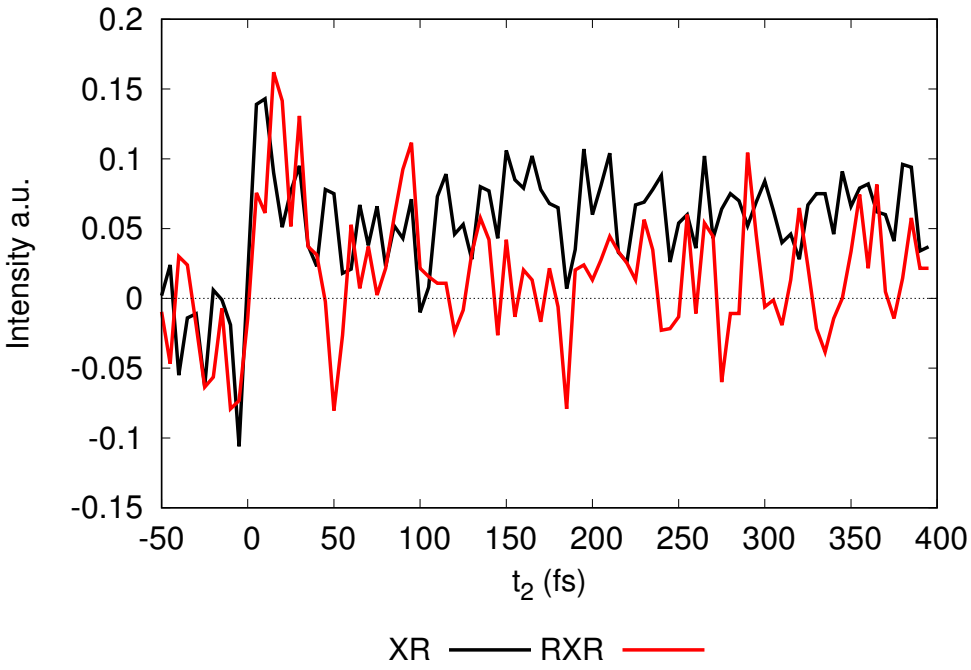

Figure S3: The time-trace of the 560 nm diagonal signal (maximum of RET absorption) for both XR (black) and RXR (red) samples. Despite the strong oscillations present in both samples, a stronger average intensity in the XR sample is observed, here interpreted as the RET absorption (present in the XR sample while absent in the RXR one).

S4 Direct/Indirect RET contribution when exciting the system at 520nm

One can argue that the signal observed at the cross-peak (520 nm,560 nm) is not EET related, but it follows from direct RET excitation: indeed, at 520 nm, the principal absorber is the CAR moiety, but there are also non negligible RET contributions (see the main text, Figure 1). In the previous Section we observed that direct RET signatures are barely detected in 2DES maps at the maximum RET absorption (560 nm diagonal), so that they will be even weaker when the sample is excited at 520 nm (where the RET absorbs less). Here we further develop this argument.

Figure 7d of the main text shows the Feynman diagrams of the possible processes occurring after population of CAR S_2. Following the Feynman rules, the RET SE diagram is weighted by the dipole factor $\langle\left(\boldsymbol{\mu}_{CAR-S_2}\cdot\hat{E}_1\right)^2\left(\boldsymbol{\mu}_{RET-S_1}\cdot\hat{E}_2\right)^2\rangle$, where $\hat{E}_1$, $\hat{E}_2$ are the polarization of the pump and probe pulses, and $\langle\bullet\rangle$ is the average over all the possible orientation of the XR protein. Similarly, direct retinal diagrams are weighted by $\langle\left(\boldsymbol{\mu}_{RET-S_1}\cdot\hat{E}_1\right)^2\left(\boldsymbol{\mu}_{RET-S_1}\cdot\hat{E}_2\right)^2\rangle$. By recalling that the experimental pulse polarization

in 2DES was set to VVHH (which implies, e.g., that $\hat{E}_1 = \hat{x}$ and $\hat{E}_2 = \hat{y}$), and that the angle between $\boldsymbol{\mu}_{RET-S_1}$ and $\boldsymbol{\mu}_{CAR-S_2}$ is $\sim 46^\circ$, one can show that the ratio between these two pre-factors (which weight direct and indirect RET contributions) is given by:

$$\frac{\langle \left(\boldsymbol{\mu}_{RET-S_1} \cdot \hat{x}\right)^2 \left(\boldsymbol{\mu}_{RET-S_1} \cdot \hat{y}\right)^2 \rangle}{\langle \left(\boldsymbol{\mu}_{CAR-S_2} \cdot \hat{x}\right)^2 \left(\boldsymbol{\mu}_{RET-S_1} \cdot \hat{y}\right)^2 \rangle} = \frac{|\boldsymbol{\mu}_{RET-S_1}|^2}{|\boldsymbol{\mu}_{CAR-S_2}|^2} \frac{9}{15} \ll 1 \tag{1}$$

because $|\boldsymbol{\mu}_{RET-S_1}|^2 < |\boldsymbol{\mu}_{CAR-S_2}|^2$.

This means that, with the VVHH pulse polarization setup employed in 2DES, energy transfer related RET contributions are stronger than direct RET signals.

S5 Tables of parameters

The theoretical modeling of the CAR signals of both XR and RXR systems has been detailed in the main text. The states included in the model are the electronic states S_0 (i.e. the ground state), S_2, S_1 and S^*. In order to describe the observed cooling of the $S_1 \rightarrow S_{1n}$ ESA signals we also introduce a hot S_1 state, called S_1^H. We assumed the CAR chromophores in both XR and RXR systems to be described by the same parameters (same energies, same transition dipoles, same transfer rates, and same coupling to the bath): the only difference between the two systems is the presence, in XR, of an additional depopulation channel, related to the EET from CAR S_2 to RET S_1.

	$\epsilon_{vertical}$ (cm^{-1})	ϵ_{0-0} (cm^{-1})	$\lvert\boldsymbol{\mu}\rvert$	angle
$S_0 \rightarrow S_2$	20975	18825	1	-
$S_1 \rightarrow S_{1n}$	16235	15730	0.96	24°
$S_1^{hot} \rightarrow S_{1n}$	15360	14750	0.96	24°
$S^* \rightarrow S_n^*$	17310	16705	0.61	24°

Table S1: Energies and transition dipoles of the Electronic Transitions involved in the Model. In the first column we report the vertical transition energy, while the second gives the adiabatic energy of the pure electronic transition. The third column gives the module of the transition dipole moments normalized to that of the $S_0 \rightarrow S_2$ transition, and the last column gives the angle of relative orientation of the transition dipole moment with respect to the $S_0 \rightarrow S_2$ transition dipole.

The energies and transition dipoles of the electronic transitions involved in the model were tuned in order to reproduce the ground-state absorption spectrum of RXR, and the 2DES maps at early times. We impose an angle of 24° between the $S_0 \rightarrow S_2$ and the S_1 (S^*) ESA transition dipole moments, as suggested by the comparison of VV and VH experimental transient spectra of xanthorhodopsin in ref. 4. The choice of the model parameters for S_1

and S^* cannot be unique, due to the limited amount of information that can be extracted from the sole experimental 2DES cuts.[3]

The coupling between the electronic transitions and intra/inter-molecular vibrations was accounted by means of spectral densities functions. The form of the spectral density was adapted from ref. 3, and the parameters tuned to fit both the RXR linear absorption spectrum and the 2DES maps. We note in particular that the intra-molecular modes, characterized by the C-C and C=C frequencies of 1150 and 1520 cm^{-1} respectively, are strongly coupled only to the $S_0 \rightarrow S_2$ transition, while they are weakly coupled to the other transitions.

$J(S_0 \rightarrow S_2)$	τ (ps)	λ (cm^{-1})	ω_c (cm^{-1})
gauss	0.020	225	–
exp_1	0.080	120	–
Vib_1	2.2	720	1150
Vib_2	2.2	1030	1520
$J(S_1 \rightarrow S_{1n})$	τ (fs)	λ (cm^{-1})	ω_c (cm^{-1})
gauss	0.020	225	–
exp_1	0.080	120	–
Vib_1	2.2	80	1150
Vib_2	2.2	80	1520
$J(S_1^H \rightarrow S_{1n})$	τ (fs)	λ (cm^{-1})	ω_c (cm^{-1})
gauss	0.020	275	–
exp_1	0.080	135	–
Vib_1	2.2	100	1150
Vib_2	2.2	100	1520
$J(S^* \rightarrow S_n^*)$	τ (fs)	λ (cm^{-1})	ω_c (cm^{-1})
gauss	0.020	275	–
exp_1	0.080	150	–
Vib_1	2.2	70	1150
Vib_2	2.2	110	1520

Table S2: Parameters for the Spectral Densities of the transitions involved in the model involved in the Model. In the table, τ denotes the relaxation time, and λ the reorganization energy of the specific part of the spectral density. For the two intra-molecular vibrations, the central frequency ω_c is given. The form of the spectral density was adapted from ref. 3.

The model includes also population dynamics described via rate equations, both from the initially excited CAR S_2 state to all the other states, and between these states. In particular, we will consider:

- The depopulation of the bright S_2 state to the dark states S_1 (S_1^H) and S^*;
- The cooling of S_1^H to S_1;
- The depopulation of S_1 and S^* to the GS S_0;

The employed transfer rate parameters are summarized in Table S3. They were adapted from ref. 4: in particular, the probabilities of branching from CAR S_2 to CAR S_1, S^* and RET S_1 were taken to be 18.5%/41.5%/40% respectively. The S_2 lifetime is different in XR and RXR systems, as in the former an additional channel, related to the EET from CAR S_2 to RET S_1 is present.

	Inverse rate
S_2-to-($S_1 + S_1^H$)	384 fs
S_2-to-S^*	170 fs
S_1^H-to-S_1	250 fs
S_1-to-S_0	2.5 ps
S^*-to-S_0	5.8 ps

Table S3: Inverse rate constants between the various states considered in the model. Adapted from ref. 4.

S6 Simulation of LA and 2DES maps

Spectra simulations were performed using a locally modified version of Spectron 2.7 [1], employing line-shape functions obtained from the spectral density to account for all dephasing mechanisms in the absence of transport, and then using the phenomenological rates (Table S3) to describe transport.

In the present system, we have assumed that the relaxation between CAR S_2 to CAR S_1 and S^* states is incoherent: this implies that the population relaxation destroys the frequency memory, and the frequency fluctuations during the first and third time period become uncorrelated. This allows to write the spectral densities of the $S_1/S^* \rightarrow S_n$ transitions in the same simple form employed for the $S_0 \rightarrow S_2$ transition, as reported in Table S2.

For the CAR S_2 transition, a (diagonal) static disorder of $\sigma = 260$ cm^{-1} was employed. The maps were obtained by averaging the results over 300 realizations of the static disorder.

S7 Normalization of the 2DES maps

The normalization procedure of experimental 2DES maps was the following: first the maximum intensity value among all the measured XR and RXR data, at each given time, was extracted. Then the maps at each time were plotted between the global maximum and its opposite (i.e. in the range [-maximum, maximum]). This allows to highlight relative differences in the two samples. Similarly, for theoretical 2DES maps, the maximum value at each given time was extracted, and the maps were plotted in the interval [-maximum, maximum].

This procedure was applied to the maps presented in Figure 3 of the main text, and also for all the maps shown in the next Section.

S8 Time resolved 2DES maps

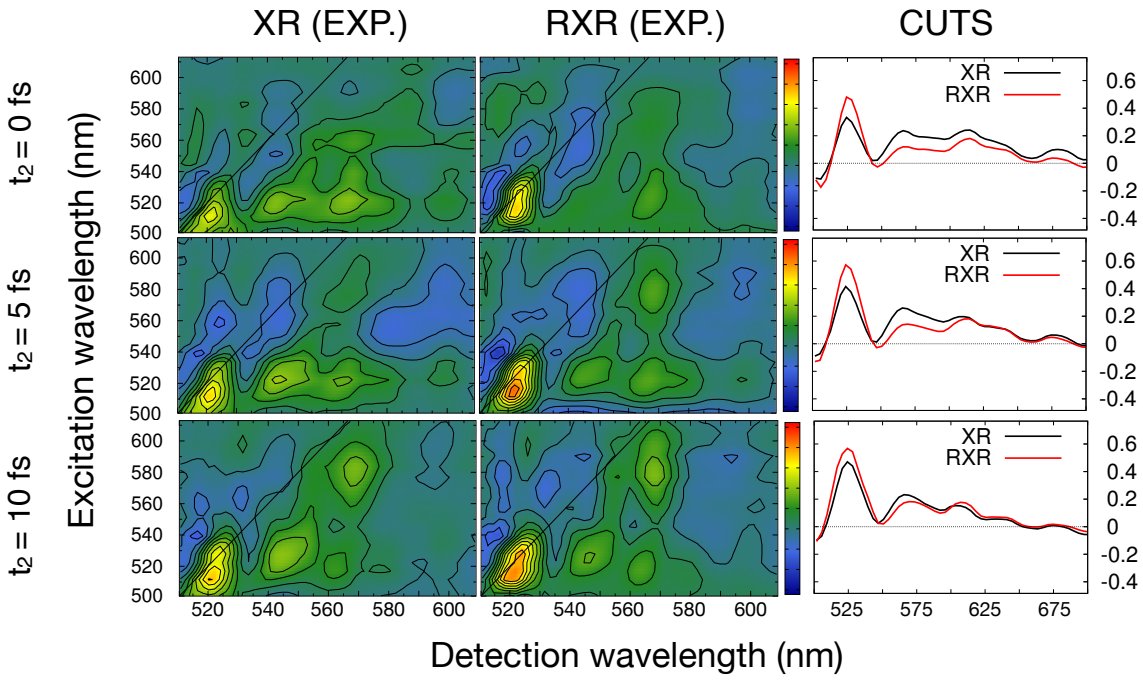

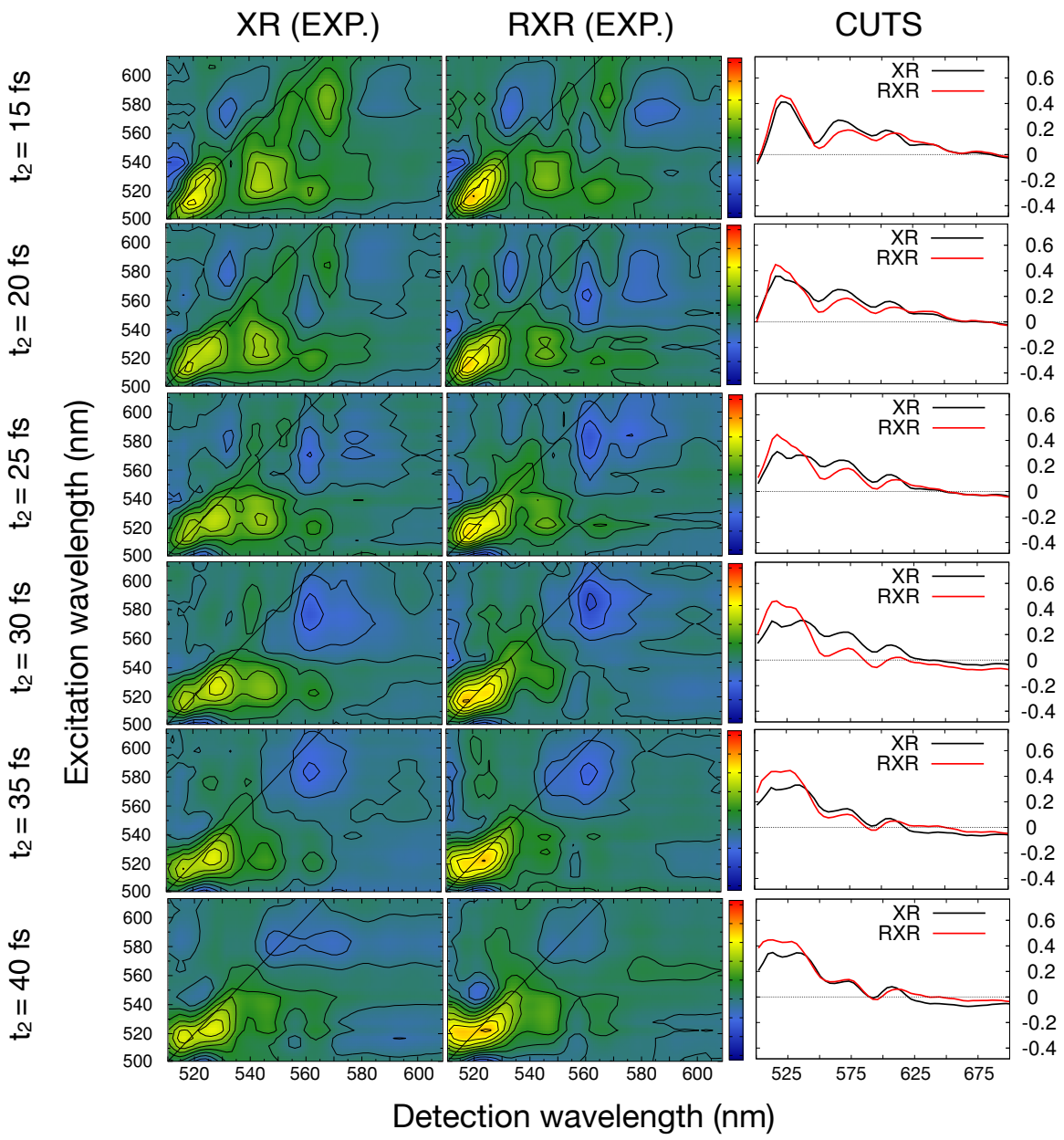
XR (EXP.)
RXR (EXP.)
CUTS
t2 = 15 fs
t2 = 20 fs
t2 = 25 fs
t2 = 30 fs
t2 = 35 fs
t2 = 40 fs
Excitation wavelength (nm)
Detection wavelength (nm)
XR
RXR

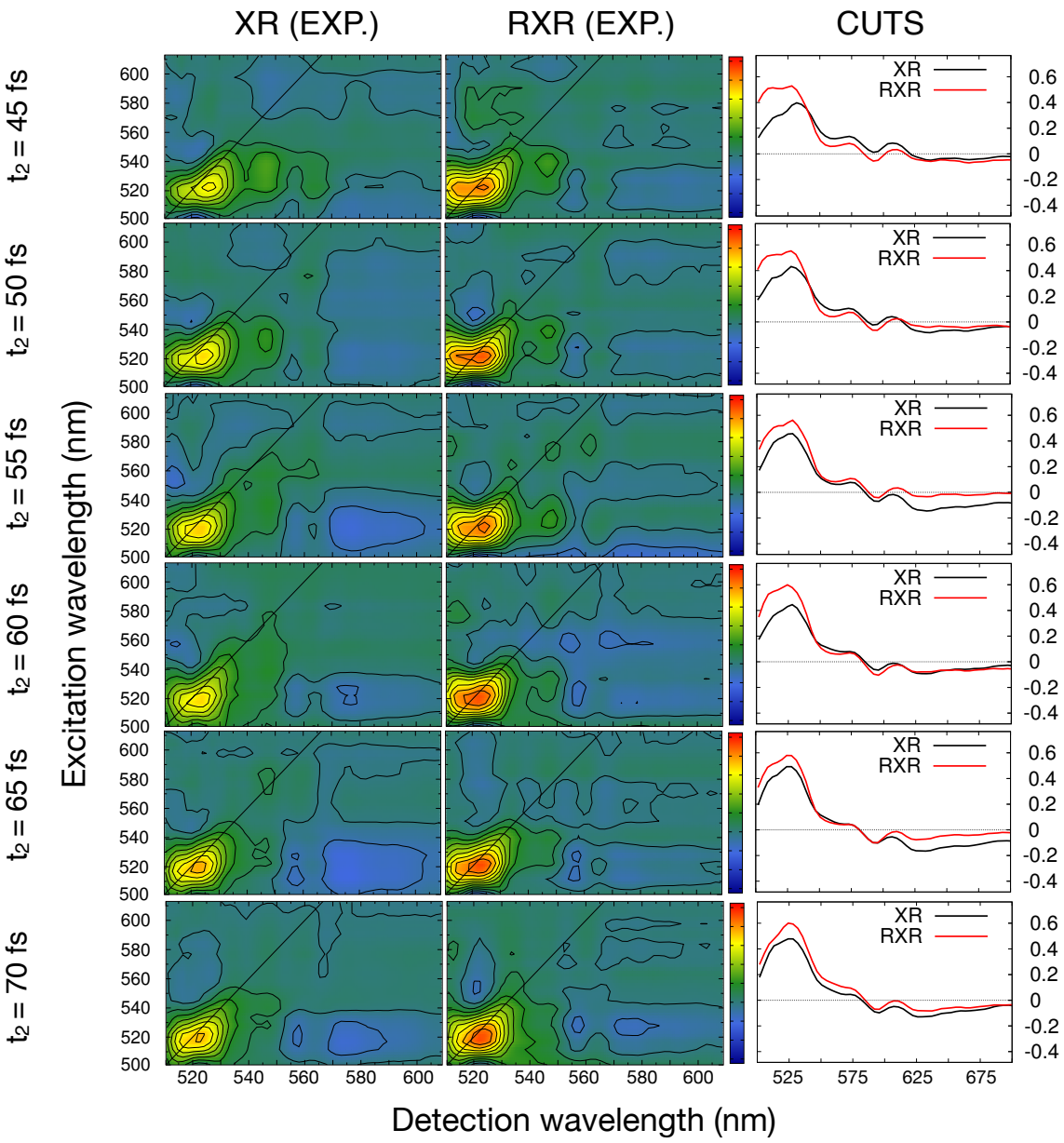
XR (EXP.)
RXR (EXP.)
CUTS
t2 = 45 fs
t2 = 50 fs
t2 = 55 fs
t2 = 60 fs
t2 = 65 fs
t2 = 70 fs
Excitation wavelength (nm)
Detection wavelength (nm)
XR
RXR

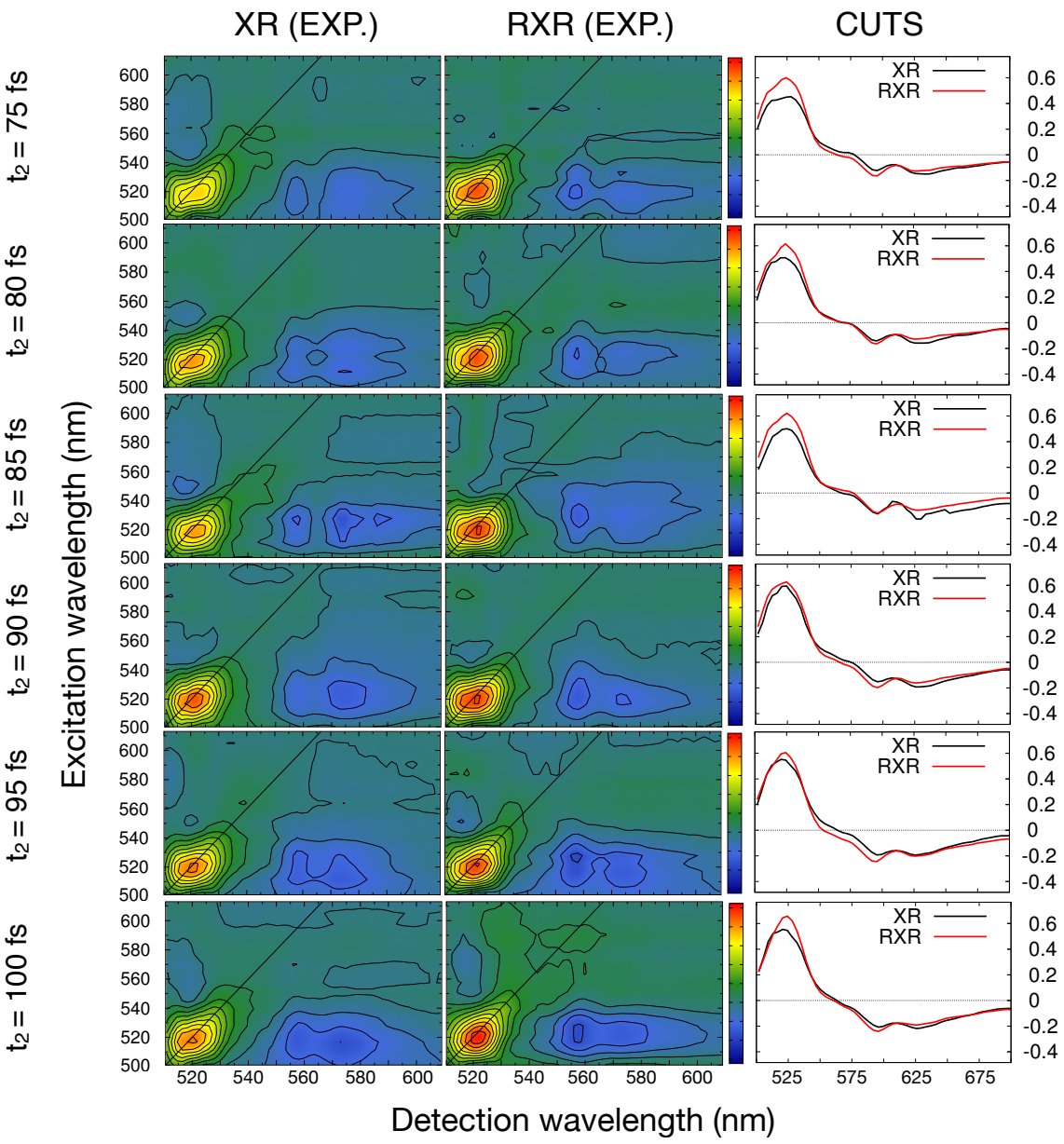
XR (EXP.)
RXR (EXP.)
CUTS
t2 = 75 fs
t2 = 80 fs
t2 = 85 fs
t2 = 90 fs
t2 = 95 fs
t2 = 100 fs
Excitation wavelength (nm)
Detection wavelength (nm)
XR
RXR

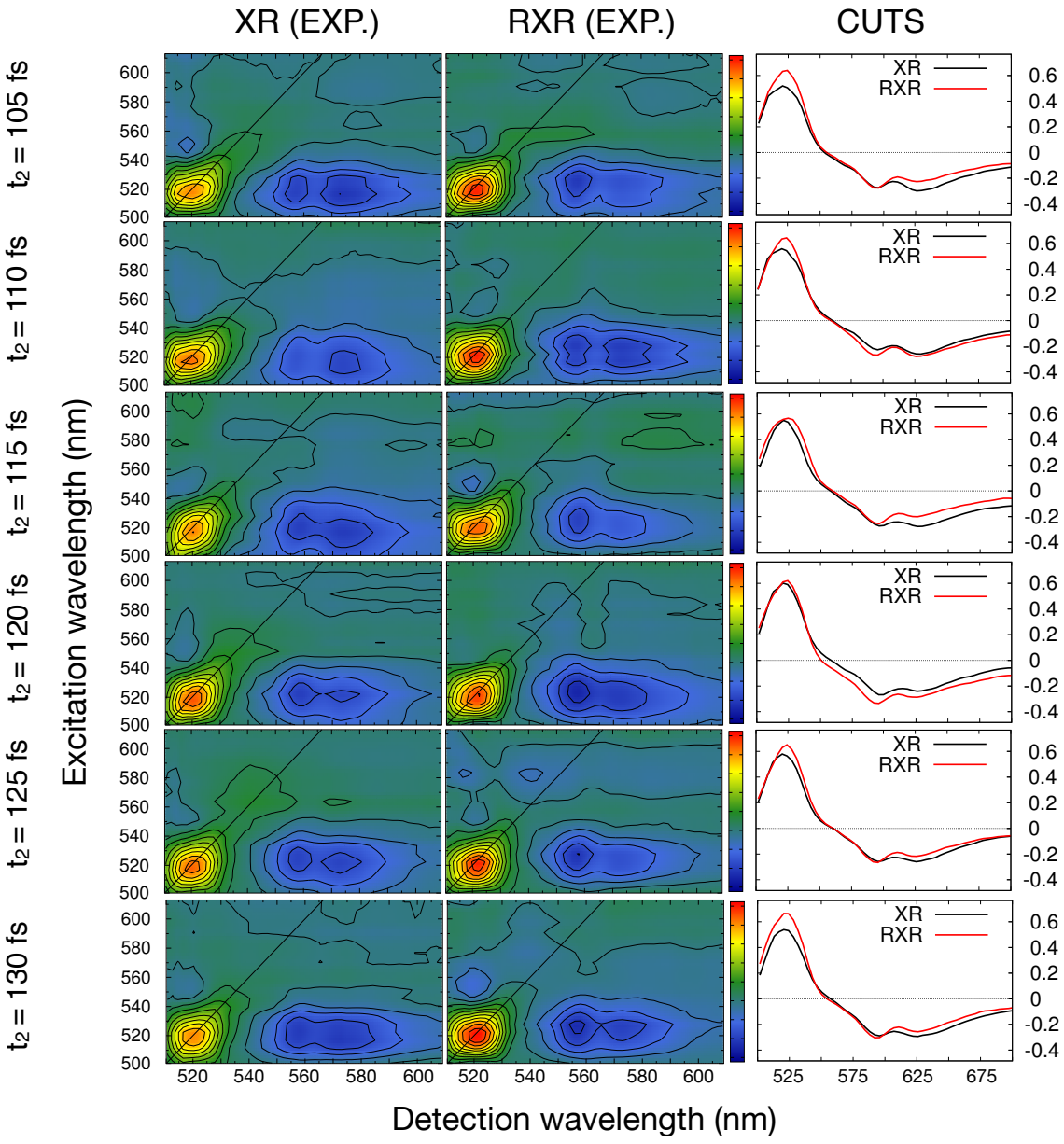
XR (EXP.)
RXR (EXP.)
CUTS
t2 = 105 fs
t2 = 110 fs
t2 = 115 fs
t2 = 120 fs
t2 = 125 fs
t2 = 130 fs
Excitation wavelength (nm)
Detection wavelength (nm)
XR
RXR

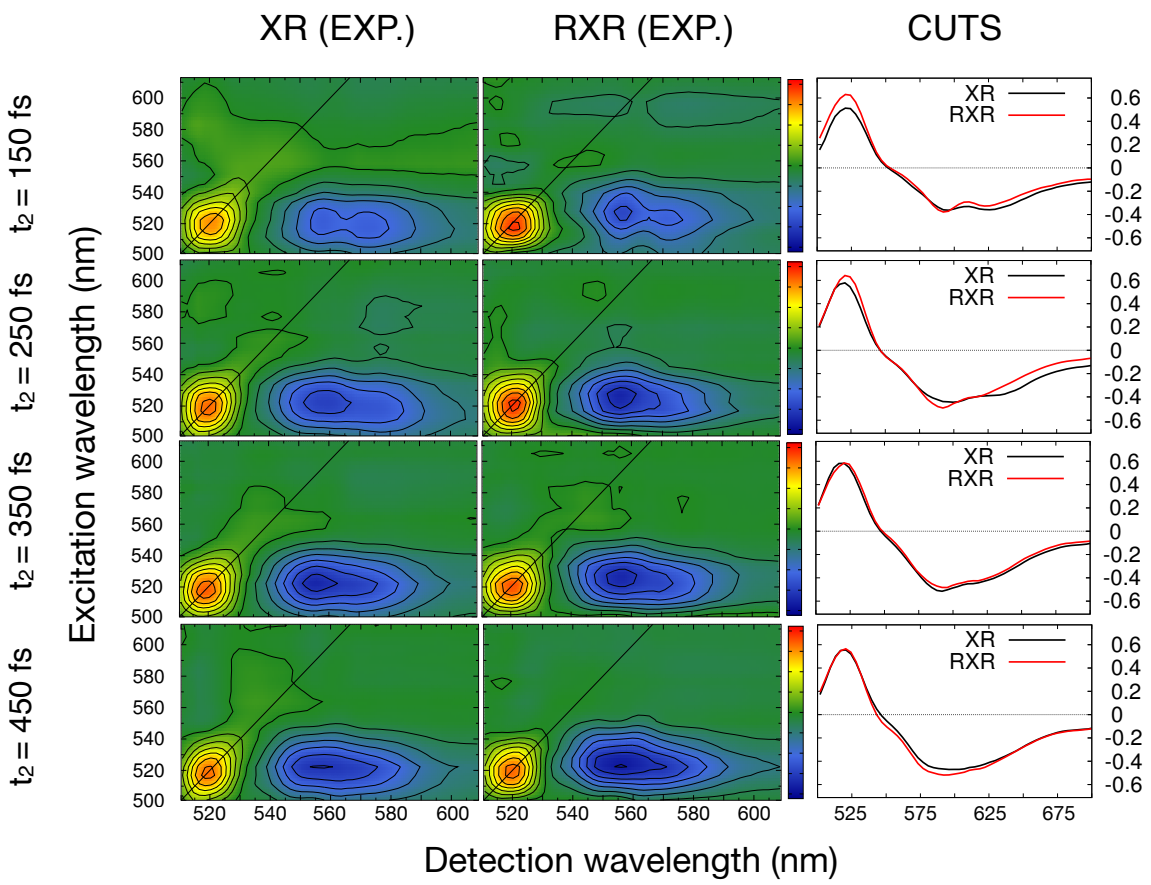
XR (EXP.)
RXR (EXP.)
CUTS
t2 = 150 fs
t2 = 250 fs
t2 = 350 fs
t2 = 450 fs
Excitation wavelength (nm)
Detection wavelength (nm)
XR
RXR

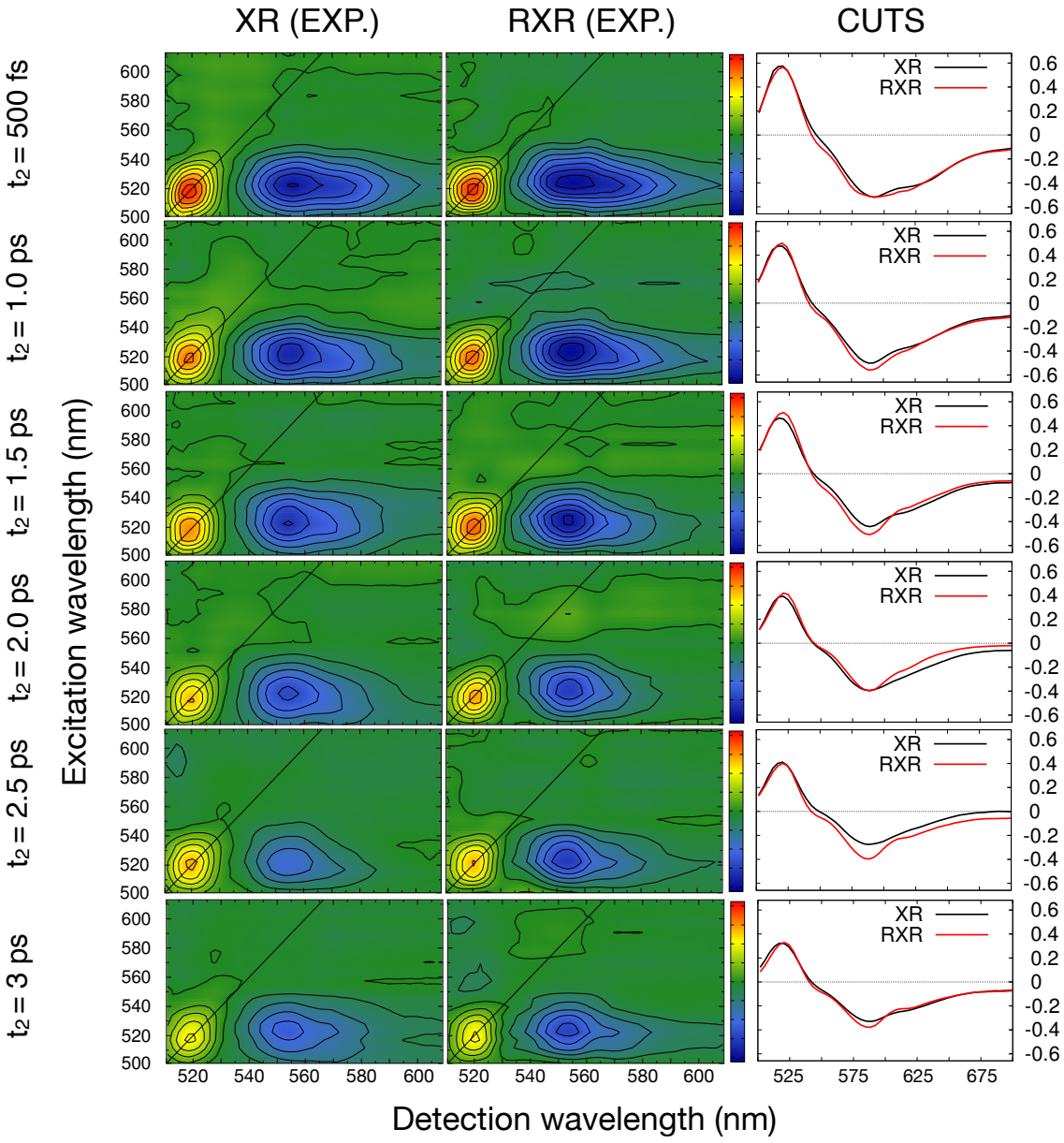
XR (EXP.)
RXR (EXP.)
CUTS
t2 = 500 fs
t2 = 1.0 ps
t2 = 1.5 ps
t2 = 2.0 ps
t2 = 2.5 ps
t2 = 3 ps
Excitation wavelength (nm)
Detection wavelength (nm)
XR
RXR

References

[1] Darius Abramavicius, Benoit Palmieri, Dmitri V. Voronine, František Šanda, and Shaul Mukamel. Coherent multidimensional optical spectroscopy of excitons in molecular aggregates; quasiparticle versus supermolecule perspectives. *Chemical Reviews*, 109(6):2350–2408, jun 2009.

[2] Sergei P. Balashov, Eleonora S. Imasheva, Jennifer M. Wang, and Janos K. Lanyi. Excitation energy-transfer and the relative orientation of retinal and carotenoid in xanthorhodopsin. *Biophysical Journal*, 95(5):2402 – 2414, 2008.

[3] Niklas Christensson, Franz Milota, Alexandra Nemeth, Jaroslaw Sperling, Harald F. Kauffmann, Tönu Pullerits, and Jürgen Hauer. Two-dimensional electronic spectroscopy of β-carotene. *The Journal of Physical Chemistry B*, 113(51):16409–16419, 2009. PMID: 19954155.

[4] Jingyi Zhu, Itay Gdor, Elena Smolensky, Noga Friedman, Mordechai Sheves, and Sanford Ruhman. Photoselective ultrafast investigation of xanthorhodopsin and its carotenoid antenna salinixanthin. *The Journal of Physical Chemistry B*, 114(8):3038–3045, 2010. PMID: 20146526.